Emergent fractional vortices and inter-layer Ising order in a bilayer of XY models

Feng-Feng Song[1] and Guang-Ming Zhang[1,2]
[1] *State Key Laboratory of Low-Dimensional Quantum Physics and Department of Physics, Tsinghua University, Beijing 100084, China.*
[2] *Frontier Science Center for Quantum Information, Beijing 100084, China.*
(Dated: May 13, 2021)

We study a bilayer system of coupled two-dimensional XY models by using tensor-network methods, showing that the inter-layer coupling can significantly alter the uncoupled topological Berezinskii-Kosterlizt-Thouless (BKT) transition. In the tensor-network representation, the partition function is mapped into a product of one-dimensional quantum transfer operator, whose eigen-equation can be accurately solved by an algorithm of matrix product states. The entanglement entropy of this one-dimensional quantum correspondence exhibits singularity, which can be used to determine various phase transitions. In the low temperature phase, an inter-layer Ising long-range order is developed, accompanying with vortex-antivortex bindings in both intra-layers and inter-layers. For two identical coupled layers, the Ising transition coincides with the BKT transition at a multi-critical point. For two inequivalent coupled layers, however, there emerges an intermediate quasi-long-range ordered phase, where vortex-antivortex bindings occur only in the layer with the larger intra-layer coupling but half-vortex pairs associated with topological strings emerge in the other layer. These results are supported by the correlation functions of the XY spins and nematic spins, and can be used to understand the novel properties in bilayer systems of superfluids, superconductors and quantum Hall systems.

Introduction. -In recent years there has been the increasing interest in a bilayer structure of coupled two-dimensional (2D) models in various physical systems, ranging from superfluids to superconductors and quantum Hall systems[1–3]. In the low temperature regime, two uncoupled layers are separately described by the phase fluctuations of a macroscopic wave function, and the vortices in the phase fields can induce the topological Berezinskii-Kosterlitz-Thouless (BKT) transition[4, 5], associated with the binding of vortices and antivortices in pairs to characterize the quantum phase coherence. Since the inter-layer Josephson couplings are relevant at low temperatures, the relative phase becomes an important degree of freedom to alter the bulk properties of the uncoupled systems significantly, and even new phases may emerge in the low temperature phases[6–10]. Due to the lack of sharp thermodynamic signatures for the BKT transition, it remains a great challenge to separate the BKT transition from its adjacent phases, which obstructs the clarification of those novel phases and their phase transitions[11–16].

Recently, tensor network methods have become a powerful theoretical tool to characterize correlated quantum many-body phases and their phase transitions in the thermodynamic limit[17, 18]. Since the partition function of a 2D statistical model can be represented as a tensor product of 1D quantum transfer operator[19], the correspondence eigen-equation can be efficiently solved by the algorithm of variational uniform matrix product states[20–23]. More importantly, the entanglement entropy of this 1D quantum correspondence exhibits singularity, corresponding to various phase transitions very precisely[24, 25]. Via such a classical-quantum correspondence, the topological BKT transition and its adjacent phase transitions in the original model can be accurately identified, and various correlation functions of local observables and the thermodynamic properties can be calculated.

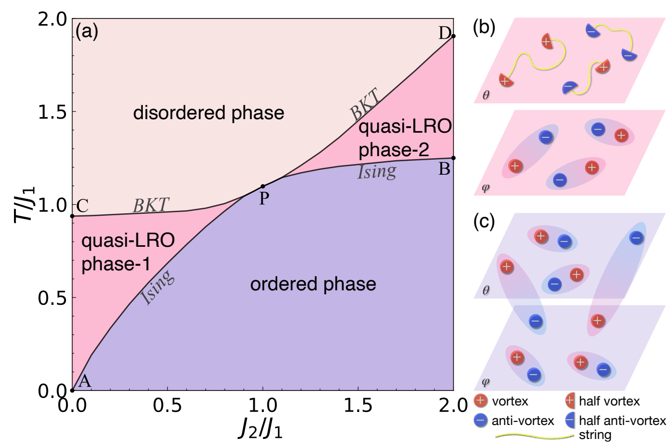

FIG. 1: (a) The complete finite-temperature phase diagram. In the low temperature phase, the inter-layer Ising-like long-range order is developed. The BKT and Ising transitions merge together at the multi-critical point P. (b) The schematic picture of the quasi-LRO phase-2. (c) The schematic picture of the low temperature ordered phase.

In this paper, we apply the tensor-network methods to the bilayer system of two-coupled XY spin models with the inter-layer nematic spin coupling, which is a generic and relevant inter-layer coupling[6]. The derived finite-temperature phase diagram is displayed in Fig.1(a). In the low-temperature phase, a local inter-layer Ising long-range order in terms of the relative phase field is developed, accompanying with the vortex-antivortex bindings in both intra-layers and inter-layers, as shown in Fig.1(c). For two identical layers, the Ising transition coincides with the BKT transition at the multi-critical point P. However, for two inequivalent layers, we have the intermediate phases with quasi-long-range order (quasi-LRO), where vortex-antivortex bindings occur only in the layer with the larger intra-layer coupling but half-vortex pairs along with their associated topological strings emerge in the other layer. Such a new type of quasi-LRO phase is supported by the two-point correlation functions of the XY spins and nematic spins, and the schematic picture is shown in Fig.1(b).

Model and tensor-network methods. -The Hamiltonian of a two-coupled XY spin model on a square lattice is defined by

$$H = -J_1 \sum_{\langle i,j \rangle} \cos(\theta_i - \theta_j) - J_2 \sum_{\langle i,j \rangle} \cos(\varphi_i - \varphi_j) + K \sum_i \cos(2\theta_i - 2\varphi_i), \quad (1)$$

where θ_i and $\varphi_i \in [0, 2\pi]$ are two $U(1)$ phase variables describing the XY spins on the upper and lower layers, respectively, J_1 and J_2 are their respective nearest-neighbour intra-layer spin interactions, and K denotes the inter-layer coupling corresponding to the second-order Josephson coupling in the experimental systems. For a general consideration, we assume $J_1 \neq J_2$, while an additional symmetry is present for $J_1 = J_2$. When $K = 0$, the model is two conventional XY spin models with two different BKT phase transitions, separating the quasi-LRO phase with vortex-antivortex pairs from the disordered phase with dissolved vortices. Due to the gapless nature of the low-temperature phase, the inter-layer coupling is always relevant for any finite value of K. In the limit of $K \to \infty$, the XY spins of the upper and lower layers are locked together, $\varphi_i = \theta_i + \pi s_i/2$ with $s_i = \pm 1$, and the model is reduced to the Ising-XY coupled model[26]: $H = -\sum_{\langle i,j \rangle}(J_1 + J_2 s_i s_j)\cos(\theta_i - \theta_j)$, which has been studied by the previous studies[27–30].

In the tensor network framework, the partition function is expressed as a contraction of local tensors defined on the original square lattice, given by

$$Z = \prod_i \iint \frac{\mathrm{d}\theta_i \mathrm{d}\varphi_i}{(2\pi)^2} \prod_{\langle i,j \rangle} \mathrm{e}^{\beta J_1 \cos(\theta_i - \theta_j)} \times \mathrm{e}^{\beta J_2 \cos(\varphi_i - \varphi_j)} \mathrm{e}^{-\beta K \cos(2\theta_i - 2\varphi_i)}, \quad (2)$$

where $\beta = 1/T$ is the inverse temperature. To obtain its tensor network representation, we apply a duality transformation that maps the phase variables on each lattice site to the number indices on the nearest-neighbor links. Such a map is achieved by the character decomposition $\mathrm{e}^{x\cos\theta} = \sum_{n=-\infty}^{\infty} I_n(x)\mathrm{e}^{in\theta}$ for each Boltzmann factor, where $I_n(x)$ is the modified Bessel function of the first kind. Then the partition function is represented as

$$Z = \prod_i \iint \frac{\mathrm{d}\theta_i \mathrm{d}\varphi_i}{(2\pi)^2} \prod_{l \in \mathcal{L}} \sum_{n_l, m_l, k_l} I_{n_l}(\beta J_1) I_{m_l}(\beta J_2) \times I_{k_l}(-\beta K) \mathrm{e}^{i n_l (\theta_i - \theta_j)} \mathrm{e}^{i m_l (\varphi_i - \varphi_j)} \mathrm{e}^{i 2 k_l (\theta_i - \varphi_i)}, \quad (3)$$

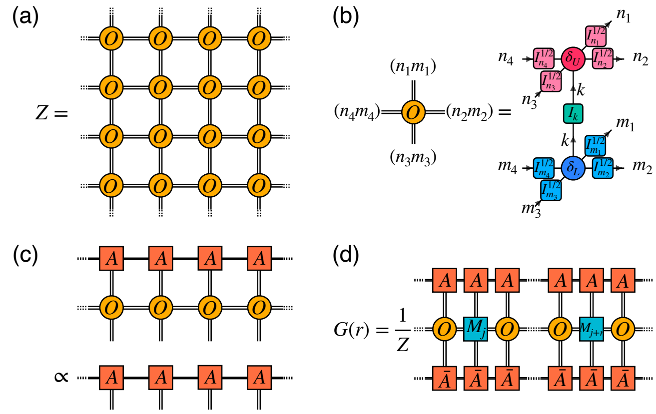

FIG. 2: (a) Tensor network representation of the partition function. (b) The construction of the local tensor O in the partition function. (c) Eigen-equation for the fixed-point uMPS $|\Psi(A)\rangle$ of the 1D quantum transfer operator T. (d) Two-point correlation function represented by contracting a sequence of channel operators.

where n_l (m_l) runs over every link on the upper (lower) layer, and k_l corresponds to every vertical link between θ_i and φ_i. By integrating out all the phase degrees of freedom, the partition function is transformed into a double tensor network (details in Supplemental Materials) as shown in Fig. 2(a)

$$Z = \mathrm{tTr} \prod_i O^{n_3 m_3, n_4 m_4}_{n_1 m_1, n_2 m_2}(i), \quad (4)$$

where "tTr" denotes the tensor contraction over all auxiliary links. As displayed in Fig. 2(b), each local tensor O is defined by

$$O^{n_3 m_3, n_4 m_4}_{n_1 m_1, n_2 m_2} = \sum_k \left(\prod_{l=1}^{4} I_{n_l}(\beta J_1) I_{m_l}(\beta J_2) \right)^{1/2} \times I_k(\beta K) \delta^{n_3+n_4}_{n_1+n_2+2k} \delta^{m_3+m_4+2k}_{m_1+m_2}, \quad (5)$$

where the inter-layer k indices are summed over and the corresponding intra-layer m_l and n_l indices are grouped together. The global $U(1)$ invariance of the bilayer model is encoded in each local tensor: $O^{n_3 m_3, n_4 m_4}_{n_1 m_1, n_2 m_2} \neq 0$ only if $n_1 + m_1 + n_2 + m_2 = n_3 + m_3 + n_4 + m_4$. Moreover, the charge conservation of each layer is reflected by $\sum_l k_l = 0$ when we make a transverse cut across all inter-layer k links. Since the expansion coefficients decrease exponentially in the Bessel function $I_n(x)$ with increasing n, an accurate truncation can be performed on the virtual indices of the local tensors.

In the tensor-network approach, the row-to-row transfer matrix composed of an infinite row of O tensors is a 1D quantum transfer operator, whose logarithmic form gives rise to a 1D quantum system with many-body interactions. Since the 1D quantum model contains complicated interactions, it had better to treat the 1D transfer matrix operator instead. Under such a correspondence, the finite-temperature properties of the 2D statistical problem are exactly mapped into a 1D quantum model at zero temperature. In the thermodynamic limit, the value of the partition function is determined by the dominant eigenvalues of the transfer operator, whose eigen-equation sketched in Fig. 2(c) is

$$T|\Psi(A)\rangle = \Lambda_{\max}|\Psi(A)\rangle, \tag{6}$$

where $|\Psi(A)\rangle$ is the leading eigenvector represented by uniform matrix product states (uMPS) made up of local A tensors[31]. This eigen-equation can be accurately solved by the algorithm of variational uniform matrix product states[20–23], which is an efficient variational method to obtain the largest eigenvector $|\Psi(A)\rangle$, corresponding to the fixed-point solution of the problem (details in Supplemental Materials). The precision of this approximation is controlled by the auxiliary bond dimension D of the local A tensors.

From the fixed-point uMPS for the 1D quantum transfer operator, various physical quantities can be estimated accurately. As far as the phase transitions in a quantum system are concerned, the quantum entanglement entropy is the most efficient measure[32], which can be directly determined via the Schmidt decomposition of $|\Psi(A)\rangle$:

$$S_E = -\sum_{\alpha=1}^{D} s_\alpha^2 \ln s_\alpha^2, \tag{7}$$

where s_α are the singular values. The two-point correlation function of the local observable h_i defined by $G(r) = \langle h_j h_{j+r}\rangle$ can be evaluated by inserting two local impurity tensors M_j and M_{j+r} into the original tensor network. With the uMPS fixed-point eigenvector, the contraction of the tensor network containing impurity tensors is reduced to a trace of an infinite sequence of channel operators

$$G(r) = \mathrm{Tr}\left(\cdots \mathbb{T}_O \mathbb{T}_{M_j} \underbrace{\mathbb{T}_O \cdots \mathbb{T}_O}_{r-1} \mathbb{T}_{M_{j+r}} \mathbb{T}_O \cdots\right). \tag{8}$$

As shown in Fig. 2(d), each channel operator has a sandwich structure $\mathbb{T}_X = \mathrm{tTr}\,(A \otimes X \otimes \bar{A})$, where $X = O, M$. Similarly, the contraction of channel operators can be determined by the leading eigenvectors of $\mathbb{T}_O$, and thus $G(r)$ is accurately obtained.

Phase Diagram. -We have noticed that the entanglement entropy S_E of the fixed-point uMPS for the 1D quantum transfer operator exhibits singularity, which provides an accurate criterion to determine the transition points. Since the inter-layer coupling is always relevant, the structure of the complete phase diagram is independent of its value, so we simply choose a practical value $K/J_1 = 0.5$ in our numerical study. To obtain the phase diagram, we have to numerically calculate the entanglement entropy under a wide range of intra-layer coupling ratios J_2/J_1. In Fig. 3(a), the entanglement entropy along $J_2/J_1 = 1.5$ develops two sharp peaks at $T_{c1} \simeq 1.21 J_1$ and $T_{c2} \simeq 1.44 J_1$, respectively. When J_2 and J_1 approach the same value, these two peaks merge together, leading to a single peak at $T_* \simeq 1.095 J_1$ as shown in Fig. 3(b). These peak positions are nearly unchanged under the bond dimensions $D = 90, 100, 110$. So the phase boundaries can be pinned down with high precision and the complete phase diagram is derived as displayed in Fig. 1(a).

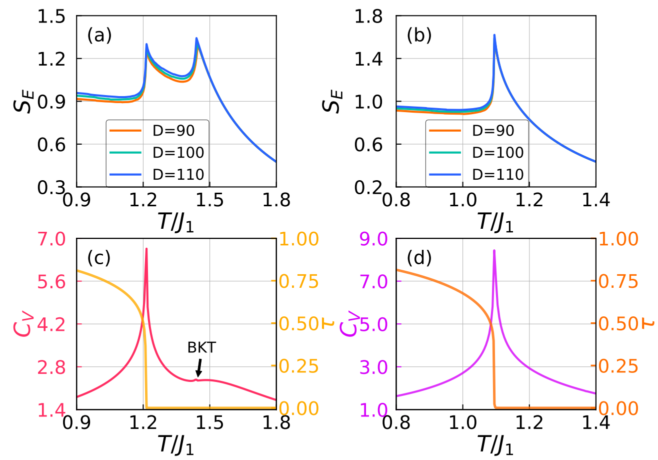

FIG. 3: (a) and (b) The entanglement entropy as a function of temperature for $J_2/J_1 = 1.5$ and $J_1 = J_2$. (c) and (d) The temperature-dependent specific heat and the inter-layer Ising order parameter along $J_2/J_1 = 1.5$ and $J_1 = J_2$, respectively.

In order to gain insight into the essential physics of different phases, we first calculate the specific heat. Within the tensor-network framework, the internal energy per site is calculated as

$$u = -2J_1\langle e^{i(\theta_j-\theta_{j+1})}\rangle - 2J_2\langle e^{i(\varphi_j-\varphi_{j+1})}\rangle + K\langle e^{i(2\theta_j-2\varphi_j)}\rangle,$$

and the specific heat is obtained by $C_V = \partial u/\partial T$. As shown in Fig. 3(c), along the line $J_2/J_1 = 1.5$, the specific heat exhibits a logarithmic divergence at T_{c1} but a small bump around T_{c2}. However, for $J_2/J_1 = 1$, a single logarithmic singularity is observed at T_* as displayed in Fig. 3(d). The logarithmic specific heat at the lower temperature reminds us of a 2D Ising phase transition with a $\mathbb{Z}_2$ symmetry breaking, while the small bump at the higher temperature indicates the nearby BKT transition.

In the presence of the inter-layer coupling, the phase fields θ and φ are no longer two independent $U(1)$ variables, and their relative phase $\sigma_i \equiv \theta_i - \varphi_i$ can be used to define a local inter-layer order parameter $\tau = \langle \sin \sigma_i \rangle$. To save the inter-layer interaction energy, the relative phase prefers to choose $\sigma_i \equiv \pm\pi/2$ as an Ising-like variable at low temperatures. As shown in Fig. 3(c) and (d), this local order parameter τ is finite below T_{c1}, indicating that an inter-layer Ising-like long-range order is established and the phase lock occurs between the XY spins in the upper and lower layers. However, when $J_2/J_1 = 1$, this Ising-like transition merges with the BKT transition at T_*, resulting in a multi-critical point P.

Correlation functions. -To further explore the nature of the quasi-LRO phases and the low-temperature ordered phase, we analyze two-point correlation functions of the local observables and their related correlation lengths. When $J_2/J_1 = 1.5$, as the temperature decreases, one transition first occurs at $T_{c2} \simeq 1.44J_1$ and then the Ising-like transition appears at $T_{c1} \simeq 1.21J_1$. In Fig. 4(a) and (b), the spin-spin correlation function $G_\varphi(r) = \langle e^{i(\varphi_j - \varphi_{j+r})} \rangle$ of the lower layer with the larger intra-layer spin coupling decays algebraically below T_{c2} but exhibits the exponential decay above T_{c2}. When approaching to T_{c2} from high temperatures, the spin correlation length ξ_φ is extracted and displayed in Fig. 4(c), and ξ_φ is well fitted by an exponentially divergent form

$$\xi(T) \propto \exp\left(\frac{b}{\sqrt{T - T_C}}\right), \quad T \to T_C^+, \tag{9}$$

where b is a non-universal positive constant. This is the characteristic BKT transition[33]. In contrast, the spin-spin correlation function of the XY spins in the upper layer $G_\theta(r) = \langle e^{i(\theta_j - \theta_{j+r})} \rangle$ decays exponentially in both the disordered phase above T_{c2} and the quasi-LRO phase below T_{c2}. The properties of the various correlation functions of the local observables in the different phases of the phase diagram are summarized in Table.1

When we focus on the quasi-LRO phase for $T_{c1} < T < T_{c2}$, there exist logarithmically interacting vortex-antivortex pairs in the lower layer with the larger inter-layer spin coupling. Meanwhile, in the upper layer with the smaller intra-layer coupling, $G_\theta(r)$ decays exponentially, but the two-point correlation function of the nematic spins exhibits an algebraic behavior,

$$G_{2\theta}(r) = \langle e^{i(2\theta_j - 2\theta_{j+r})} \rangle \sim r^{-\eta_{2\theta}}, \tag{10}$$

as shown in Fig. 4(d) and (e). Such a behavior indicates that the integer vortices in the upper layer are fractionalized into half-integer vortex pairs due to the presence of the inter-layer squared cosine interaction. Since the half-integer vortices are point singularities around which spin directions rotate through an angle π on circumnavigation, each pair of half-vortices should be connected by a topological string across which spins are antiparallel[34–37]. If the integer vortex-antivortex pairs are regarded

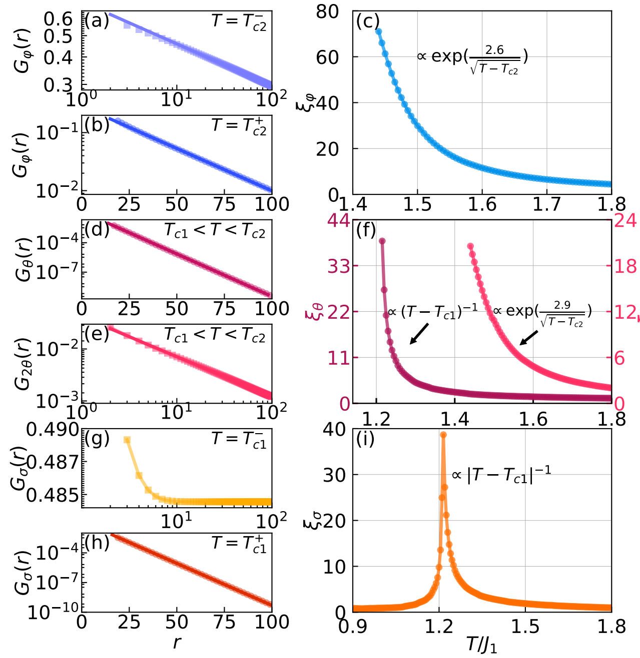

FIG. 4: Various two-point correlation functions are calculated for $J_2/J_1 = 1.5$. (a) and (b) The spin-spin correlation function of the lower layer at $T/J_1 = 1.3$ and $T/J_1 = 1.5$. (c) The spin correlation length in the lower layer above T_{c2}. (d) and (e) Correlation functions of the XY spins and nematic spins in the upper layer at $T/J_1 = 1.3$. (f) The corresponding spin and nematic spin correlation lengths of the upper layer. (g) and (h) Correlation functions of the inter-layer Ising variable at $T/J_1 = 1.1$ and 1.3. (i) The correlation length of the inter-layer Ising variable.

as a quasi-LRO condensate of the Cooper pairs in 2D superfluids, the half-integer vortex pairs may be viewed as a quasi-LRO condensate of pairs of the Cooper pairs[38].

Further investigations on the characteristic correlation lengths of the spins in the upper layer can provide a deeper understanding. As shown in Fig. 4(f), it is found that the nematic-spin correlation length $\xi_{2\theta}$ has an exponentially divergent behavior, indicating that the BKT phase transition of the half-integer vortex bindings happens exactly at T_{c2}. For $T_{c1} < T < T_{c2}$, the spin correlation length ξ_θ diverges as $(T - T_{c1})^{-1}$ as the same as the 2D Ising transition. Below T_{c1}, the spin-spin correlation functions of both the intra-layer $G_\theta(r)$ and the inter-layer $G_{\theta\varphi}(r) = \langle e^{i(\theta_j - \varphi_{j+r})} \rangle$ display the algebraic behavior, implying the vortex-antivortex bindings in both intra-layers and inter-layers, a fully phase-coherent state of the bilayer system.

In fact, the Ising transition and the BKT transition are closely related to each other. To elucidate this point, we calculate the correlation function of the local Ising variable σ_j defined by $G_\sigma(r) = \langle \mathrm{e}^{i(\sigma_j - \sigma_{j+r})} \rangle$. As depicted in Fig. 4(g) and (h), we found that $G_\sigma(r)$ converges to a nonzero constant in the large distance limit below T_{c1},

TABLE I: Various correlation functions in the different phases of the phase diagram.

	Disordered	quasi-LRO-1	quasi-LRO-2	Ordered
$\langle e^{i(\varphi_i-\varphi_j)}\rangle$	$\sim e^{-r/\xi_\varphi}$	$\sim e^{-r/\xi_\varphi}$	$\sim r^{-\eta_\varphi}$	$\sim r^{-\eta_\varphi}$
$\langle e^{i2(\varphi_i-\varphi_j)}\rangle$	$\sim e^{-r/\xi_{2\varphi}}$	$\sim r^{-\eta_{2\varphi}}$	$\sim r^{-\eta_{2\varphi}}$	$\sim r^{-\eta_{2\varphi}}$
$\langle e^{i(\theta_i-\theta_j)}\rangle$	$\sim e^{-r/\xi_\theta}$	$\sim r^{-\eta_\theta}$	$\sim e^{-r/\xi_\theta}$	$\sim r^{-\eta_\theta}$
$\langle e^{i2(\theta_i-\theta_j)}\rangle$	$\sim e^{-r/\xi_{2\theta}}$	$\sim r^{-\eta_{2\theta}}$	$\sim r^{-\eta_{2\theta}}$	$\sim r^{-\eta_{2\theta}}$
$\langle e^{i(\theta_i-\varphi_j)}\rangle$	$\sim e^{-r/\xi_{\theta\varphi}}$	$\sim e^{-r/\xi_{\theta\varphi}}$	$\sim e^{-r/\xi_{\theta\varphi}}$	$\sim r^{-\eta_{\theta\varphi}}$
$\langle e^{i(\sigma_i-\sigma_j)}\rangle$	$\sim e^{-r/\xi_\sigma}$	$\sim e^{-r/\xi_\sigma}$	$\sim e^{-r/\xi_\sigma}$	$\sim$ const.

but an exponential decay above T_{c1}. The convergent behavior is consistent with the formation of a long-range order of the σ_j inter-layer Ising spins. Moreover, as shown in Fig. 4(i), the correlation length ξ_σ of the inter-layer Ising variables diverges as $|T - T_{c1}|^{-1}$. Furthermore, when $J_2/J_1 = 1$, the Ising transition coincides with the BKT transition exactly at the multi-critical point, where there is an interplay between the Ising and BKT degrees of freedom at the microscopic level and exhibits a new universality class of critical properties with emerged supersymmetry[39].

Conclusion. -We have used the tensor-network methods to study the bilayer system of two-coupled 2D XY spin models. The complete finite-temperature phase diagram has been accurately determined. In the low-temperature phase, the relative phase field forms a long-range Ising-like order, accompanying with the vortex-antivortex bindings in both intra-layers and inter-layers. In two inequivalent coupled XY spin models, the emergence of half-integer vortex pairs in one layer with the smaller intra-layer coupling coexists with the integer vortex-antivortex pairs in the other layer with the larger intra-layer spin coupling, giving rise to the unusual intermediate temperature phases with quasi-LRO. To the best of our knowledge, it is the first time to find such a phase diagram for a bilayer system.

It should be pointed out that the inter-layer Ising symmetry of the bilayer system can be related to the time-reversal symmetry. When the relative phase is locked in the low-temperature order phase, the corresponding superfluids or superconductors display the time-reversal symmetry breaking. Actually such a phase has been observed in the layered superconductors with two different superconducting pairing order parameters[40, 41]. Since the half-integer vortex pairs may be associated with the pairs of Cooper pairs in the absence of phase coherence among the Cooper pairs[42, 43], the quasi-LRO phases with unusual properties are deserved by future experimental investigations.

Acknowledgments. The authors are indebted to Qi Zhang for his stimulating discussions and earlier collaboration. The research is supported by the National Key Research and Development Program of MOST of China (2017YFA0302902).

[1] F. Tafuri and J. R. Kirtley, Reports on Progress in Physics **68**, 2573 (2005), URL https://doi.org/10.1088/0034-4885/68/11/r03.
[2] V. Karle, N. Defenu, and T. Enss, Phys. Rev. A **99**, 063627 (2019), URL https://link.aps.org/doi/10.1103/PhysRevA.99.063627.
[3] J. P. Eisenstein, Annual Review of Condensed Matter Physics **5**, 159 (2014), 1306.0584.
[4] V. Berezinsky, Sov. Phys. JETP **32**, 493 (1971).
[5] J. M. Kosterlitz and D. J. Thouless, Journal of Physics C: Solid State Physics **6**, 1181 (1973), URL https://doi.org/10.1088.
[6] E. Granato and J. M. Kosterlitz, Phys. Rev. B **33**, 4767 (1986), URL https://link.aps.org/doi/10.1103/PhysRevB.33.4767.
[7] T. A. Bojesen, E. Babaev, and A. Sudbø, Phys. Rev. B **88**, 220511 (2013), URL https://link.aps.org/doi/10.1103/PhysRevB.88.220511.
[8] G. Bighin, N. Defenu, I. Nándori, L. Salasnich, and A. Trombettoni, Phys. Rev. Lett. **123**, 100601 (2019), URL https://link.aps.org/doi/10.1103/PhysRevLett.123.100601.
[9] M. Zeng, L.-H. Hu, H.-Y. Hu, Y.-Z. You, and C. Wu, arXiv e-prints arXiv:2102.06158 (2021), 2102.06158.
[10] V. Drouin-Touchette, P. P. Orth, P. Coleman, P. Chandra, and T. C. Lubensky, arXiv e-prints arXiv:2103.01878 (2021), 2103.01878.
[11] R. Gupta, J. DeLapp, G. G. Batrouni, G. C. Fox, C. F. Baillie, and J. Apostolakis, Phys. Rev. Lett. **61**, 1996 (1988), URL https://link.aps.org/doi/10.1103/PhysRevLett.61.1996.
[12] R. Gupta and C. F. Baillie, Phys. Rev. B **45**, 2883 (1992), URL https://link.aps.org/doi/10.1103/PhysRevB.45.2883.
[13] M. Hasenbusch, Journal of Physics A: Mathematical and General **38**, 5869 (2005), URL https://doi.org/10.1088/0305-4470/38/26/003.
[14] H. Arisue, Phys. Rev. E **79**, 011107 (2009), URL https://link.aps.org/doi/10.1103/PhysRevE.79.011107.
[15] Y. Komura and Y. Okabe, Journal of the Physical Society of Japan **81**, 113001 (2012), https://doi.org/10.1143/JPSJ.81.113001, URL https://doi.org/10.1143/JPSJ.81.113001.
[16] Y.-D. Hsieh, Y.-J. Kao, and A. W. Sandvik, Journal of Statistical Mechanics: Theory and Experiment **2013**, P09001 (2013), URL https://doi.org/10.1088.
[17] F. Verstraete, V. Murg, and J. Cirac, Advances in Physics **57**, 143 (2008), https://doi.org/10.1080/14789940801912366, URL https://doi.org/10.1080/14789940801912366.
[18] R. Orús, Annals of Physics **349**, 117 (2014), ISSN 0003-4916, URL http://www.sciencedirect.com/science/article/pii/S0003491614001596.
[19] J. Haegeman and F. Verstraete, Annual Review of Condensed Matter Physics **8**, 355 (2017), https://doi.org/10.1146/annurev-conmatphys-031016-025507, URL https://doi.org/10.1146/annurev-conmatphys-031016-025507.

[20] V. Zauner-Stauber, L. Vanderstraeten, M. T. Fishman, F. Verstraete, and J. Haegeman, Phys. Rev. B **97**, 045145 (2018), URL https://link.aps.org/doi/10.1103/PhysRevB.97.045145.

[21] M. T. Fishman, L. Vanderstraeten, V. Zauner-Stauber, J. Haegeman, and F. Verstraete, Phys. Rev. B **98**, 235148 (2018), URL https://link.aps.org/doi/10.1103/PhysRevB.98.235148.

[22] L. Vanderstraeten, J. Haegeman, and F. Verstraete, SciPost Phys. Lect. Notes p. 7 (2019), URL https://scipost.org/10.21468/SciPostPhysLectNotes.7.

[23] L. Vanderstraeten, B. Vanhecke, A. M. Läuchli, and F. Verstraete, Phys. Rev. E **100**, 062136 (2019), URL https://link.aps.org/doi/10.1103/PhysRevE.100.062136.

[24] Z.-Q. Li, L.-P. Yang, Z. Y. Xie, H.-H. Tu, H.-J. Liao, and T. Xiang, Phys. Rev. E **101**, 060105 (2020), URL https://link.aps.org/doi/10.1103/PhysRevE.101.060105.

[25] F.-F. Song and G.-M. Zhang, Phys. Rev. B **103**, 024518 (2021), URL https://link.aps.org/doi/10.1103/PhysRevB.103.024518.

[26] M. Y. Choi and S. Doniach, Phys. Rev. B **31**, 4516 (1985), URL https://link.aps.org/doi/10.1103/PhysRevB.31.4516.

[27] E. Granato, J. M. Kosterlitz, J. Lee, and M. P. Nightingale, Phys. Rev. Lett. **66**, 1090 (1991), URL https://link.aps.org/doi/10.1103/PhysRevLett.66.1090.

[28] J. Lee, E. Granato, and J. M. Kosterlitz, Phys. Rev. B **44**, 4819 (1991), URL https://link.aps.org/doi/10.1103/PhysRevB.44.4819.

[29] M. S. Li and M. Cieplak, Phys. Rev. B **50**, 955 (1994), URL https://link.aps.org/doi/10.1103/PhysRevB.50.955.

[30] M. P. Nightingale, E. Granato, and J. M. Kosterlitz, Phys. Rev. B **52**, 7402 (1995), URL https://link.aps.org/doi/10.1103/PhysRevB.52.7402.

[31] V. Zauner-Stauber, L. Vanderstraeten, M. T. Fishman, F. Verstraete, and J. Haegeman, Phys. Rev. B **97**, 045145 (2018), URL https://link.aps.org/doi/10.1103/PhysRevB.97.045145.

[32] G. Vidal, J. I. Latorre, E. Rico, and A. Kitaev, Phys. Rev. Lett. **90**, 227902 (2003), URL https://link.aps.org/doi/10.1103/PhysRevLett.90.227902.

[33] J. M. Kosterlitz, Journal of Physics C: Solid State Physics **7**, 1046 (1974), URL https://doi.org/10.1088.

[34] D. H. Lee and G. Grinstein, Phys. Rev. Lett. **55**, 541 (1985), URL https://link.aps.org/doi/10.1103/PhysRevLett.55.541.

[35] D. B. Carpenter and J. T. Chalker, Journal of Physics: Condensed Matter **1**, 4907 (1989), URL https://doi.org/10.1088.

[36] Y. Shi, A. Lamacraft, and P. Fendley, Phys. Rev. Lett. **107**, 240601 (2011), URL https://link.aps.org/doi/10.1103/PhysRevLett.107.240601.

[37] P. Serna, J. T. Chalker, and P. Fendley, Journal of Physics A: Mathematical and Theoretical **50**, 424003 (2017), URL https://doi.org/10.1088.

[38] B. Douçot and J. Vidal, Phys. Rev. Lett. **88**, 227005 (2002), URL https://link.aps.org/doi/10.1103/PhysRevLett.88.227005.

[39] L. Huijse, B. Bauer, and E. Berg, Phys. Rev. Lett. **114**, 090404 (2015), URL https://link.aps.org/doi/10.1103/PhysRevLett.114.090404.

[40] S. K. Ghosh, M. Smidman, T. Shang, J. F. Annett, A. D. Hillier, J. Quintanilla, and H. Yuan, Journal of Physics Condensed Matter **33**, 033001 (2021), 2003.04357.

[41] V. Grinenko, R. Sarkar, K. Kihou, C. H. Lee, I. Morozov, S. Aswartham, B. Büchner, P. Chekhonin, W. Skrotzki, K. Nenkov, et al., Nature Physics **16** (2020).

[42] E. Berg, E. Fradkin, and S. A. Kivelson, Nature Physics **5**, 830 (2009).

[43] R. M. Fernandes and L. Fu, arXiv e-prints arXiv:2101.07943 (2021), 2101.07943.